Health-conscious optimization for long-term operation of a green hydrogen production plant

Federico Del Mondo[a], Marco Russo Cirillo[a], Davide Pivetta[a], Marco Bogar[a], Rodolfo Taccani[a]

[a] Department of Engineering and Architecture, University of Trieste, 34127 Trieste, Italy
federico.delmondo@dia.units.it (CA), marco.russocirillo@phd.units.it, dpivetta@units.it, marco.bogar@dia.units.it, taccani@units.it

Abstract:
This work presents a system-level Mixed-Integer Linear Programming (MILP) framework for the long-term operational optimization of a commercial-scale green hydrogen production plant integrating photovoltaic (PV) generation, Battery Energy Storage System (BESS), Proton Exchange Membrane Water Electrolyzer (PEMWE), hydrogen compression, and storage. The methodology is applied to the hydrogen production plant currently under implementation in Trieste within the North Adriatic Hydrogen Valley (NAHV) initiative and is developed over a time horizon of 87,600 h. The proposed framework minimizes the specific operational cost of hydrogen production while accounting for BESS ageing and evaluating PEMWE degradation.
Two operating scenarios are investigated: Scenario 1 considers a fixed hydrogen production target of 1000 kg/day with flexible grid support through a Power Purchase Agreement (PPA), whereas Scenario 2 aims at maximizing daily hydrogen production with a constant PPA electricity supply. Results show that the operating strategy has a higher influence on both hydrogen cost and component ageing. Scenario 2 requires a more intensive use of the BESS to operate the PEMWE closer to its efficiency region and has a higher dependence on grid electricity characterized by an higher unit cost. As a consequence, the BESS lifetime in Scenario 1 is approximately 25% higher than in Scenario 2, leading to an estimated LCOE difference of about 3% between the two cases. Moreover, Scenario 2 shows an average annual hydrogen operational cost about 6.2% higher than Scenario 1, due to the greater reliance on grid electricity and lower efficiency operational processes.
No significant difference is observed in the cost increase associated with degradation between the two Scenarios as them are characterized by similar daily hydrogen production levels.

Keywords:
Green hydrogen; Water electrolysis, Degradation, long-term operation.

1. Introduction

Green hydrogen production through water electrolysis is increasingly recognized as a key technology for decarbonizing energy systems.mHowever, the widespread deployment of electrolysis-based hydrogen production is still constrained by the limited energy efficiency, performance losses and the high costs, highlighting the need for advanced digital tools to support long-term operational planning .
Although Proton Exchange Membrane Water electrolyzers (PEMWE) have significantly advanced in recent years, their large-scale deployment is still affected by efficiency losses and degradation mechanisms that progressively increase cell voltage and reduce stack lifetime[1].
Intermittent renewable supply, frequent start–stop cycles, and load variations can further accelerate ageing phenomena and influence the long-term techno-economic performance of the hydrogen production plants. Therefore, understanding degradation phenomena of electrolyzers operating under dynamic conditions is crucial for the deployment of future green hydrogen markets [2].
Some techno-economic studies of large-scale electrolysis systems have identified electricity purchasement, utilization factor, and operating strategies as major drivers of green hydrogen cost, thereby motivating the adoption of optimization-based tools for electrolyzer scheduling and plant management [3].
As for example, in [4] it is highlighted that assuming a PEMWE partial-load strategy instead of fixed load the hydrogen average cost can be decreased up to 17% thereby demonstrating the importance of MILP-based approach in accounting for the efficiency behaviour of electrolysis systems. A recent study [5] reports that the cost of electricity can account more than 64% of the total Levelized Cost of Hydrogen (LCOH), emphasizing the effect of operational strategy and reliance on grid electricity on the overall economic viability of green hydrogen production. Moreover in [6] it is pointed out that many optimization studies on renewable-coupled PEMWE systems still neglect the impact of degradation on operating efficiency, despite that performance

losses affect specific energy consumption, component lifetime and, consequently, the overall techno-economic performance of the system. The authors in [7] have identified that accounting for degradation in LCOH calculation can underestimate the cost from 2 to 10 % depending on the degradation rates considered, thus demonstrating that neglecting the performance decay may underestimate the hydrogen production cost.
This work proposes a system-level Mixed Integer Linear Programming (MILP) optimization framework for a long-term operation of a commercial-scale hydrogen production plant integrating water electrolysis, aimed at minimizing operational hydrogen production costs considering also performance losses over a specific hydrogen production time horizon of 87,600 hours.
The proposed methodology is applied to the hydrogen production facility currently under implementation in Trieste within the North Adriatic Hydrogen Valley (NAHV).
The daily plant operation is optimized to ensure that the PEMWE, supported by the Battery Energy Storage System (BESS), operates in a regime that minimizes hydrogen production operating costs, while BESS state of health (SOH_{BESS}) and PEMWE degradation are explicitly accounted for within the overall assessment framework. This establishes a preliminary framework for quantifying the effect of degradation on the final hydrogen cost and provides a basis for future optimization approaches in which the degradation minimization is directly treated as an additional objective function.
In particular, two plant operating Scenarios are investigated:

- Scenario 1, based on a fixed hydrogen production target of 1000 kg_{H2}/day, with a flexible Power Purchase Agreement (PPA) allowing grid electricity imports of up to 2 MWh in order to meet the daily production target;
- Scenario 2, based on maximizing the hydrogen production achievable by the PEMWE, with a fixed PPA supply equal to 2 MWh, such that the daily hydrogen production is determined by the combined contribution of PV generation and the constant grid import.

Therefore, the novelty of this work lies in the development of a more realistic framework for the long-term operational planning of PEMWE systems, integrating efficiency variations, degradation-related performance losses, and the operational strategy based on the PPA contract.

2. Methodology

2.1. Energy system description

The simplified energy system shown in Figure 1 represents the configuration of a power-to-hydrogen plant currently being implemented in Trieste within the framework of the NAHV initiative [8].

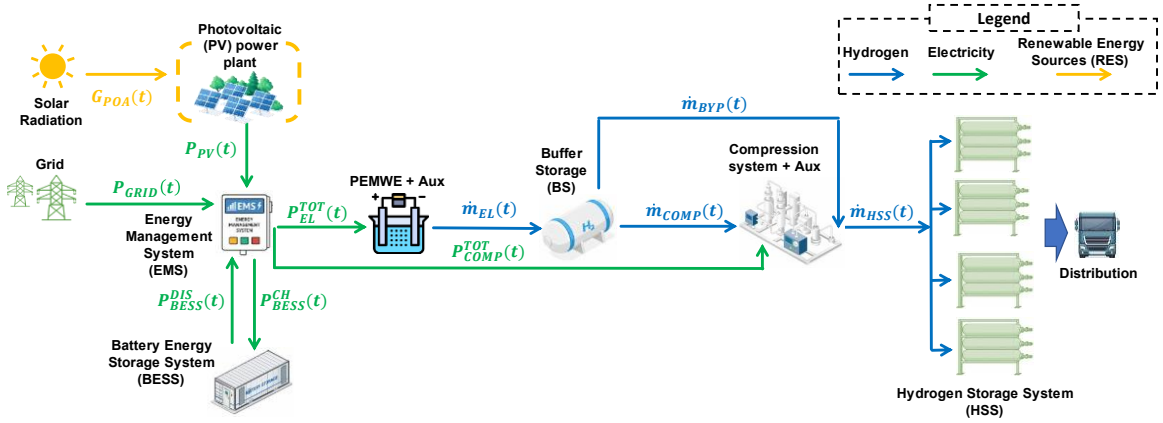

Figure 1: *Schematic layout of the hydrogen production plant currently under implementation in Trieste as part of the North Adriatic Hydrogen Valley (NAHV) initiative.*

The hydrogen production plant includes on-site electricity generation from a photovoltaic (PV) system, renewable grid electricity supplied under a Power Purchase Agreement (PPA), a Battery Energy Storage System (BESS), a Proton Exchange Membrane Water Electrolyzer (PEMWE), a compression system composed by two multi-stage compressors, a Hydrogen Storage System (HSS); the hydrogen is then distributed in gaseous form by truck trailers. In addition, the overall plant operation is supported by auxiliary systems, which are not explicitly depicted in Figure 1 but are included in the plant modelling.

The plant energy supply is regulated by an Energy Management System (EMS), which controls and dispatches electricity from the PV system and the grid to the plant subsystems enhancing flexible plant operation.
Whenever the available PV power is insufficient to meet the instantaneous plant demand, electricity from the grid is used as a supplementary source to ensure continuous operation and to meet the hydrogen production target in Scenario 1 or as a constant supplementary energy input in Scenario 2.
The EMS also determines whether the available electricity should be stored or directly used, thus enabling the PEMWE to operate within its optimal efficiency range. This operating logic is consistent with the non-linear efficiency behaviour of PEMWE, for which the maximum system efficiency is generally achieved at partial load rather than at nominal operation [9].
Table 1 reports the nominal capacities for the subsystems of the considered hydrogen production plant, which define the overall sizing of the system considered in this study.

Table 1: *Nominal capacities for the subsystems of the considered hydrogen production plant.*

Coefficient	Description	Unit	Value
P_{PV}^{MAX}	PV system capacity	MWp	5
E_{BESS}^{MAX}	BESS capacity	MWh	2
P_{EL}^{MAX}	PEMWE capacity	MW	5
$P_{AUX(EL)}$	PEMWE auxiliary systems capacity	MW	0.1*P_{EL}^{MAX}
P_{COMP}^{MAX}	Nominal compressor power	kW	110
$P_{AUX(COMP)}$	Compressors auxiliary systems power	kW	0.1*$P_{AUX(COMP)}$
V_{HSS}^{MAX}	Maximum HSS storage capacity	ton	2
p_{TR}^{MAX}	Maximum distribution trailer pressure	bar	200
p_{TR}^{RES}	Residual trailer pressure	bar	20
V_{TR}^{MAX}	Maximum distribution trailer volume	m3	28

2.1. Energy system operation

The PV electrical power output P_{PV} represents the power produced by the local PV. In addition, the hydrogen plant can import green electricity from the grid with a power equal to P_{GRID}through a PPA.
The BESS is used to mitigate the effects of PV intermittency and to modulate the power supplied to the PEMWE throughout the day. The BESS charging and discharging processes are affected by efficiency losses; accordingly, the effective charging and discharging power rates are represented by P_{BESS}^{CH} and P_{BESS}^{DIS}, respectively.
The PEMWE system is assumed to achieve the maximum efficiency at 35% of its nominal load, whereas the minimum operating power is set at 20% of nominal power, as operation below this threshold is associated with lower production efficiency and is therefore neglected at the system level as reported in [10].
The electrical power required by the PEMWE system P_{EL}^{TOT} accounts for the operating stack power P_{EL} and the operating power required by the PEMWE auxiliary systems $P_{AUX(EL)}$.
The compression system requires a total electrical power P_{COMP}^{TOT}, defined as the sum of the electrical power absorbed by the compressor P_{COMP} and the power demand of the associated auxiliary systems $P_{AUX(COMP)}$. To ensure stable and efficient compressor operation despite variability in hydrogen production, a buffer storage (BS) system is located upstream of the compressor in order to guarantee a regulated hydrogen mass flow rate at the compressor inlet.
Hydrogen loading to HSS can occur under either (i) free-loading and/or (ii) forced-loading conditions. In free-loading mode, hydrogen is transferred directly from the BS to the HSS with a mass flow rate $\dot{m}_{\mathrm{BYP}}$ by exploiting the pressure gradient between the upstream BS and the downstream HSS, without additional mechanical work.
In forced-loading mode, hydrogen from the BS is compressed, and the resulting mass flow rate corresponds to the hydrogen processed by the compressor $\dot{m}_{\mathrm{COMP}}$. The compressed hydrogen is then transferred to the HSS, with a resulting mass flow rate equal to $\dot{m}_{\mathrm{HSS}}$. From the HSS the hydrogen is then filled within the truck trailers mainly under free loading conditions.
The storage operating scenario considered within the modelling approach corresponds to the minimum HSS residual pressure p_{HSS}^{RES} (typically between 150 and 200 bar), that allows the storage of the daily hydrogen production in an HSS characterized by a maximum pressure of p_{HSS}^{MAX}. The filling of the truck trailers is assumed to take place under free-loading conditions and is therefore not explicitly considered in the model.
The main parameters regarding plant operations are reported in Table 2.

Table 2: *Main parameters regarding plant operation.*

Coefficient	Description	Unit	Value
E_{BESS}^{MAX}	BESS nominal capacity	MWh	2
P_{BESS}^{MAX}	Maximum input/output BESS power	MW	1
P_{GRID}^{MAX}	Maximum grid import power	MW	2
E_{GRID}^{MAX}	Maximum grid import energy	MWh	2
$\dot{m}_{H2_{EL}}^{MAX}$	PEMWE nominal hydrogen production rate	kg/h	90
p_{HSS}^{MAX}	Maximum storage pressure	bar	500
p_{HSS}^{RES}	Residual pressure	bar	≈200
p_{COMP}^{IN}	Compressor inlet pressure	Pa	$30 \cdot 10^5$
$P_{AUX(PL)}^{MAX}$	Plant auxiliary systems power	kW	50
P_{EL}^{STB}	PEMWE standby power needs	kW	50

2.3. Modelling

The system ageing is evaluated over a time horizon of 87,600 hours and the P_{PV} is obtained through the PVGIS tool [11], considering as a reference period the 2013-2022 years interval and the PV plant specific characteristics [12]. The cost of energy produced by the PV system is evaluated using the Levelized Cost of Energy (LCOE) metric, which provides a representative unit cost for PV generation over the system lifetime. The LCOE, is obtained by using the formulation reported in [13], through the economic and technical parameters reported in Table 3. The resulting value is equal to 75 €/MWh, in line with [14].

Table 3: *Economic and technical parameter of the PV system.*

Parameter	Unit	Value	Source
PV system investment cost	€/kWp	450	[15]
BESS investment cost	€/kWh	2000	[16]
Site development and infrastructure costs	€/kWp	350	[17]
Discount rate	%	5	-
Mean PV production	MWh/y	6500	[11]
PV modules rep. cost	€/kWp	250	[18]
PV Modules O&M cost	€/kW/y	10	[19]
Modules lifetime	y	30	[20]
Panel degradation	%/y	0.4	
BESS rep cost	€/kWh	630	[13]
O&M cost	€/kWh/y	20	[21]
BESS lifetime	y	15	

In both Scenarios, the cost of electricity purchased through the PPA, c_{GRID}, is assumed to be fixed at 150 €/MWh throughout the analysis and represents the cost of green electricity supplied by the grid whenever local PV generation is insufficient to meet the hydrogen production target of 1000 kg_{H2}/day in Scenario 1, or as a constant supplementary energy input in Scenario 2.

For the BESS, the charging and discharging efficiencies, respectively η_{BESS}^{ch} and η_{BESS}^{dis} respectively, are included in Eqs. (1) and (2) to account for conversion losses and ensure a realistic representation of battery operation, in accordance with [22]. Where, C_{rate} is the parameter that express the rate at which a BESS it is charged or discharged relative to its nominal capacity, with a C_{rate} equal to 1 indicating the battery is fully charged or discharged in one hour.

$$\eta_{BESS}^{ch} = 0.9912 - 0.0422 \cdot C_{rate} + 0.0082 \cdot C_{rate}^2 \quad (1)$$

$$\eta_{BESS}^{dis} = 0.9972 - 0.0413 \cdot C_{rate} + 0.0034 \cdot C_{rate}^2 \quad (2)$$

Therefore, P_{BESS}^{CH} is obtained by multiplying $\eta_{BESS}^{ch}$with the electrical power supplied to the BESS during the charging process P_{BESS}^{IN} and P_{BESS}^{DIS} is obtained by multiplying η_{BESS}^{dis} with the electrical power supplied by the BESS during the discharging process P_{BESS}^{OUT}.

Moreover, P_{BESS}^{IN} and P_{BESS}^{OUT} are characterized by a maximum power rating of 1 MW and the admissible range of the BESS state of charge SoC_{BESS} is considered between 0 and 2 MWh at the Beginning of Life (BoL) for modelling purposes.
The PEMWE efficiency η_{EL} and hydrogen production rate $\dot{m}_{EL}$ curves, are defined based on the experimental data of the PEMWE, showing a maximum efficiency of 65% at 35% of the nominal PEMWE load and a minimum efficiency of 58.5% at nominal load. When the PEMWE operates in standby mode - i.e., with no hydrogen production but remaining in a controlled state to enable a rapid return to operation - an additional electrical power demand P_{EL}^{STB} is required to maintain the operating temperature and pressure of the electrolysis system [23].
The PEMWE cell electrochemical model is developed in line with [24] and the cell voltage V_{cell} at PEMWE BoL is expressed as the sum of the open-circuit voltage V_{OCV}, the activation overvoltage $V_{activation}$ and the ohmic overvoltage V_{ohmic}.

$$V_{cell} = V_{OCV} + V_{activation} + V_{ohmic} \ [V] \tag{3}$$

The PEMWE design parameters, including the number of stacks, the number of cells per stack, and the cell active area (Table 4), are taken from the literature [25] [26] and used to extend the cell-level electrochemical model to the PEMWE system considered in this work. From the PEMWE power consumption and hydrogen production rate at each operating point, the corresponding efficiency curve at PEMWE BoL is determined.
In order to calibrate the obtained efficiency curve with the experimental data, a calibration step has been introduced, by using the ionic resistance as a fitting parameter as introduced in [27]. The value of this parameter has been selected to limit the deviation between the calculated curve and the experimental one to less than 2% for operating powers above 20% of the nominal power, as this portion of the curve is the most representative for the considered application as considered in Section 2.1.

***Table 4**: Main PEMWE design parameters considered in the electrochemical model.*

Design parameter	Unit	Value
PEMWE number of stacks	-	5
Number of cells per stack	-	126
Cell Area	cm^2	1250

Regarding the PEMWE auxiliary systems (e.g.: cooling system, water pump, etc) $P_{AUX(EL)}$ is modelled as a term proportional to P_{EL} and reaching its maximum value $P_{AUX(PL)}^{MAX}$ at P_{EL}^{MAX}.
The compression system has been modelled following the methodology presented in [28]. The compressor specific power consumption SEC_{COMP}, mainly depends on the pressure increase required to compress hydrogen from the residual storage pressure, p_{HSS}^{RES}, to the maximum storage pressure, p_{HSS}^{MAX}.
For both scenarios, although the residual storage pressure is expected to vary in order to accommodate the full hydrogen production as introduced in Section 2.1, the compressor specific energy consumption, SEC_{COMP}, is assumed constant and equal to 1.85 kWh/kg. This assumption is adopted to isolate the difference between the two operational strategies as mainly resulting from the electrolyzer efficiency, while still accounting for the share of electrical energy required for hydrogen compression.
The auxiliary power consumption of the compressor system $P_{AUX(COMP)}$ is modelled as a linear function of the $\dot{m}_{H2_{COMP}}$ processed by the compressor. Specifically, the auxiliary power scales proportionally with $\dot{m}_{H2_{COMP}}$, and its maximum admissible value $\dot{m}_{H2_{COMP}}^{MAX}$, reaching the maximum auxiliary power $P_{AUX(COMP)}^{MAX}$ at nominal compressor operation. The total electrical power consumption of the plant auxiliary systems $P_{AUX(PL)}^{TOT}$ (e.g.: water treatment unit, monitoring devices, etc) is modelled as a term proportional to P_{EL}^{TOT} and reaching its maximum value $P_{AUX(PL)}^{MAX}$ at P_{EL}^{MAX}.

2.4. Optimization and degradation evaluation framework

The following section presents the mathematical formulation adopted for the minimization of hydrogen production cost. The resulting Mixed-Integer Linear Programming (MILP) problem is implemented in the Python programming language and solved using the Gurobi optimizer [29] . All operational variables and constraints are defined over a discrete time horizon $t \in T = \{1, \dots, 24\}$ with an hourly resolution (Δt equal to 1).
Within the proposed framework, BESS degradation is directly incorporated into the optimization through the progressive reduction in available battery capacity, while PEMWE degradation is accounted for through the time-dependent update of electrolyzer performance, enabling the evaluation of its effect on system operation.

Objective function

The objective function, Eq. (8), is defined to minimize the specific operational cost of hydrogen production, expressed in €/kgH2, through the optimal management of energy sources, conversion units, and storage systems.

$$f_{obj} = \frac{\min \sum_{t \in T} (\mathrm{P_{PV,dir}(t) \cdot c_{PV}} + \mathrm{P^{IN}_{BESS(PV)}(t) \cdot c_{PV}} + \mathrm{P^{IN}_{BESS(GRID)}(t) \cdot c_{GRID}} + \mathrm{P_{GRID,dir}(t) \cdot c_{GRID}}) \cdot \Delta t}{\mathrm{H2_{prod,day}}} \quad (8)$$

In Eq. (8), the coefficients c_{PV} (equal to LCOE) and c_{GRID} represent the unit costs of electricity supplied by the photovoltaic system and the electrical grid (€/KWh), respectively, while the corresponding power terms account for the direct and storage-mediated energy contributions over the optimization horizon. $P_{PV,dir}(t)$ represents the photovoltaic power directly supplied to the hydrogen production plant, $P^{IN}_{BESS(\mathrm{PV})}(t)$ represents the photovoltaic power used to charge the BESS. Similarly, $P_{GRID,dir}(t)$ indicates the grid power directly consumed by the hydrogen production plant, $P^{IN}_{BESS(\mathrm{GRID})}(t)$ corresponds to the grid power used for BESS charging.

The PEMWE and BESS efficiency curves and the PEMWE hydrogen production curve, exhibiting non-linear behavior, are approximated using piecewise linear (PWL) functions.

The PEMWE hydrogen production rate $\dot{m}_{H2_{EL}}$ is approximated by a PWL function $f_{el}(\cdot)$ defined over a set of breakpoints as introduced Eq. (5).

$$\dot{m}_{H2_{EL}}(\mathrm{t}) = \mathrm{f}_{el}(P_{EL}(t), \eta_{EL}(\mathrm{t})) \quad (5)$$

In which $P^{TOT}_{EL}(t)$ is the sum of $P_{EL}(t)$, $P^{STB}_{EL}(t)$, and $P_{AUX(EL)}(t)$.

BESS charging and discharging processes are also characterized by efficiencies losses. The electrical energy effectively stored in BESS or supplied by the BESS is therefore modeled using PWL functions, respectively $g_{ch}(\cdot)$ and $g_{dis}(\cdot)$ as presented in Eq.(6) and Eq. (7).

$$P^{CH}_{BESS}(\mathrm{t}) = g_{ch}(\mathrm{P^{IN}_{BESS}(t)}, \eta^{ch}_{BESS}(\mathrm{t})) \quad (6)$$

$$P^{DIS}_{BESS}(\mathrm{t}) = g_{dis}(\mathrm{P^{OUT}_{BESS}(t)}, \eta^{dis}_{BESS}(\mathrm{t})) \quad (7)$$

The total compressor power demand $\mathrm{P^{TOT}_{COMP}(t)}$ includes both $P_{COMP}(t)$, assumed to scale linearly with SEC_{COMP} coefficient, and $P_{AUX(COMP)}$ to scale proportionally with $\dot{m}_{H2_{COMP}}(t)$, as expressed in Eq. (8).

$$\mathrm{P^{TOT}_{COMP}(t)} = SEC_{COMP} \cdot \dot{m}_{H2_{COMP}}(t) + P^{MAX}_{AUX(COMP)} \cdot \frac{\dot{m}_{H2_{COMP}}(t)}{\dot{m}^{MAX}_{H2_{COMP}}} \quad (8)$$

The MILP formulation accounts for the plant auxiliary systems and $P^{TOT}_{AUX(PL)}(t)$, calculated through Eq. (9).

$$P^{TOT}_{AUX(PL)}(t) = P^{MAX}_{AUX(PL)} \cdot \frac{P_{EL}(t)}{P^{MAX}_{EL}} \quad (9)$$

Constraints

The power balance Eq. (10), ensures that the total power demand of the PEMWE, compressor and auxiliary systems, meets the available power from PV system, BESS, and grid supply.

$$P^{TOT}_{EL}(\mathrm{t}) + P^{TOT}_{COMP}(\mathrm{t}) + P^{TOT}_{AUX(PL)}(\mathrm{t}) = \mathrm{P_{PV,dir}(t)} + \mathrm{P^{DIS}_{BESS}(t)} + \mathrm{P_{GRID,dir}(t)} \quad (10)$$

To prevent multiple start–stop cycles within the day, a monotonicity constraint is introduced in the PEMWE operation through the binary variable $\tau(t)$ Eq.(11). These constraints ensure that the PEMWE can be switched on at most once during the day.

$$\tau(t) \geq \tau(t-1) \quad (11)$$

The status of PEMWE operation is regulated by Eq. (12) that ensures electrolyzer operation within its technical power limits when is switched on.

$$\mathrm{P^{MIN}_{EL}(t)} \cdot \tau(t) \leq P_{EL} \leq \mathrm{P^{MAX}_{EL}(t)} \cdot \tau(t) \quad (12)$$

The electrical power demand of the PEMWE during standby operation is modelled through Eq. (13), where the parameter a represents the auxiliary power required to maintain the system in standby conditions (a equal to 50 kW).

$$\mathrm{P}_{EL}^{STB}(t) = a \cdot (1 - \tau(t)) \tag{13}$$

The electrical power needed for the standby operations is represented by the sum of the portion supplied by the grid $\mathrm{P}_{EL(Grid)}^{STB}(t)$ or by PV system $\mathrm{P}_{EL(PV)}^{STB}(t)$, Eq. (14).

$$\mathrm{P}_{EL}^{STB}(t) = \mathrm{P}_{EL(PV)}^{STB}(t) + \mathrm{P}_{EL(Grid)}^{STB}(t) \tag{14}$$

Total BESS input power P_{BESS}^{IN} is decomposed into contributions from PV generation and grid electricity Eq. (15), while Eq. (16) ensures that the BESS charging power remains below P_{BESS}^{MAX}.

$$P_{BESS(PV)}^{IN}(\mathrm{t}) + P_{BESS(PV)}^{IN}(\mathrm{t}) = P_{BESS}^{IN}(\mathrm{t}) \tag{15}$$

$$P_{BESS,IN}^{PV}(\mathrm{t}) + P_{BESS,IN}^{GRID}(\mathrm{t}) \leq P_{BESS}^{MAX} \tag{16}$$

The BESS output power as for the input power is constrained according to Eq. (17).

$$P_{BESS}^{OUT}(\mathrm{t}) \leq P_{BESS}^{MAX} \tag{17}$$

Eq. (18) ensures that the energy produced by the PV system is equal to the sum of the energy supplied to the BESS or directly used by the hydrogen plant.

$$P_{PV,dir}(t) + P_{BESS(PV)}^{IN}(t) = P_{PV}(t) \tag{18}$$

The BESS can be charged also by the energy supplied from the grid. Differently from the PV case, where the entire generated energy is directly utilized or stored in the BESS, the optimizer determines the amount of electricity requested from the grid up to P_{GRID}^{MAX} as presented in Eq. (19) and Eq. (20).

$$P_{GRID,dir}(t) + P_{BESS(GRID)}^{IN}(t) \leq P_{GRID}(t) \tag{19}$$

$$P_{GRID}(t) \leq P_{GRID}^{MAX}(t) \tag{20}$$

When the grid supply is active the constrain presented in Eq. (21) enforces a strictly positive grid power import with ϵ.

$$P_{GRID}(t) \geq \epsilon \cdot \theta(t) \forall t \tag{21}$$

The BESS SoC is updated based on the energy charged into or discharged from the BESS, as expressed in Eq. (22).

$$SoC(t) = SoC(t-1) + P_{BATT}^{ch} \cdot \Delta\mathrm{t} - P_{BATT}^{dis} \cdot \Delta\mathrm{t} \tag{22}$$

The BESS SoC is explicitly initialized at the beginning of the optimization horizon by imposing $SoC(1) = 0$ and $SoC(2) = 0$. These constraints define a fully discharged BESS at the start of the scheduling horizon and during the first step. This assumption, ensures physical consistency of the energy balance, and allows the subsequent evolution of the BESS SoC to be driven exclusively by charging and discharging decisions within the modeled horizon.

The BESS SoC is constrained as presented in Eq. (23): where SoC^{MIN} is equal to E_{BESS}^{MIN} and the upper bound is represented by the BESS State of Healt (SOH_{BESS}) that is equal to E_{BESS}^{MAX} at the BoL.

$$SoC^{MIN} \leq SoC(t) \leq SOH_{BESS} \tag{23}$$

The progressive reduction over time in the maximum BESS capacity, represented by SOH_{BESS}, results from ageing associated with battery charge-discharge cycling and is described by Eq. (24) according to [30], where the equivalent number of full charge-discharge cycles (EFC) is evaluated using the Rainflow counting method reported in [31].

$$SOH_{BESS} = SOH_{BESS(day-1)} - \frac{EFC_{day}}{5200 \cdot (\Delta soc)_{day}^{-1.5}} \tag{24}$$

The battery charge - discharge logic Eq. (25) and Eq. (26) ensures that the battery cannot charge and discharge simultaneously and it is governed by the binary variable $\sigma(t)$.

$$P_{BESS}^{IN}(t) \leq P_{BESS}^{MAX}(t) \cdot \sigma(t) \tag{25}$$

$$P_{BESS}^{OUT}(t) \leq P_{BESS}^{MAX}(t) \cdot (1 - \sigma(t)) \quad (26)$$

To guarantee optimal operation of the hydrogen compression system, a lower bound on $\dot{m}_{H2_{EL}}$ is introduced, as expressed by the constraint reported in Eq. (27), where $m_{H2_{BS}}$ represents the hydrogen mass stored in the BS system.

$$\dot{m}_{H2_{EL}}(t) + \dot{m}_{H2_{BESS}}(\mathrm{t}) \geq \dot{m}_{H2_{COMP}}^{MIN}(t) \quad (27)$$

The daily hydrogen production requirement is defined according to the considered operating scenario as reported in Eq. (28). For Scenario 1, the total daily hydrogen production is constrained to match the assigned target, $H2_{TARGET}^{DAY}$. In Scenario 2, instead, the daily hydrogen production, $H2^{DAY}$, is determined by the available energy resources.

$$\sum_{t \in T} \dot{m}_{H2_{EL}}(t) = \begin{cases} H2_{TARGET}^{DAY} & \text{for Scenario 1} \\ H2^{DAY} & \text{for Scenario 2} \end{cases} \quad (28)$$

From a practical modelling perspective, Scenario 2 is implemented by imposing a sufficiently high daily hydrogen production target, so that the optimization problem is not effectively constrained by the target itself and returns the maximum hydrogen production achievable during the day under the available electrical energy conditions. In this context, the MILP optimization remains necessary to define the hourly energy balances and to determine the operating behaviour of the BESS.

Starting from the determined $P_{EL}(t)$, that not includes the degradation effects, the electrochemical cell operating point represented by the cell voltage $V_{cell(op)}(t)$ and the current density $i_{cell(op)}(t)$ is determined through Eq. (3).

The PEMWE cell voltage increase due to degradation phenomena is recalculated at each time step by considering the formulation introduced in Eq. (29) [32] in which $\Delta V_{cell,deg}$ is the additional term introduced to account for the progressive voltage increase associated with the degradation over time Eq.(30).

$$V_{cell,deg} = V_{OCV} + V_{activation} + V_{ohmic} + \Delta V_{cell,deg} \ \ [V] \quad (29)$$

$$\Delta V_{cell,deg} = \left(0.2499 \cdot i_{op} + 2.3545\right) \cdot 10^{6} \ \ [V/h] \quad (30)$$

Starting from $\boldsymbol{i_{cell(op)}(t)}$ the corresponding degraded cell voltage, $V_{cell(op),deg}$, is determined and then used to calculate $\boldsymbol{P_{EL,deg}(t)}$, representing the effective PEMWE power requirement under degraded conditions.

3. Results

This section presents the main results of the long-term optimization framework applied to the commercial-scale hydrogen production plant considered in this study. The analysis aims to assess the impact of different plant operating strategies on hydrogen production plant performances and hydrogen production cost over a time horizon of 87,600 hours, while accounting for the progressive effects of BESS and PEMWE degradation. In particular the proposed approach enables the quantification of the techno-economic effects of PEMWE efficiency, dependance on grid electricity and systems degradation under different operating Scenarios conditions.

In particular, the analysis is developed by considering two operating Scenarios:

- Scenario 1, based on a fixed hydrogen production target of 1000 kgH2/day, with a flexible Power Purchase Agreement (PPA) arrangement allowing grid electricity imports of up to 2 MWh in order to meet the daily production target;
- Scenario 2, based on maximizing the hydrogen production achievable by the PEMWE, with a fixed PPA supply equal to 2 MWh, such that the daily hydrogen production is determined by the combined contribution of PV generation and the constant grid import.

In this study, the BESS is assumed to reach end-of-life (EoL) when its remaining capacity decreases to 70% of the nominal value, in line with commonly adopted thresholds reported in the literature for lithium-ion batteries and BESS [33].

Th e adopted empirical cycle-aging relationship assumes that BESS lifetime decreases with increasing cycling depth: deeper charge-discharge cycles lead to a lower number of achievable equivalent full cycles, whereas shallower cycles allow the battery to withstand a higher number of cycles before reaching end-of-life.

Figure 2 illustrates the evolution of BESS degradation from BoL over the analyzed time horizon and shows that the estimated BESS lifetime is approximately 25% higher in Scenario 1 than in Scenario 2.

The results also show that an optimization strategy focused exclusively on maximizing the operational efficiency of the electrolysis system can lead to substantial BESS degradation.

Figure 2: *Battery degradation over the considered time horizon of ten years for Scenario 1 and Scenario 2 of hydrogen plant operation strategy.*

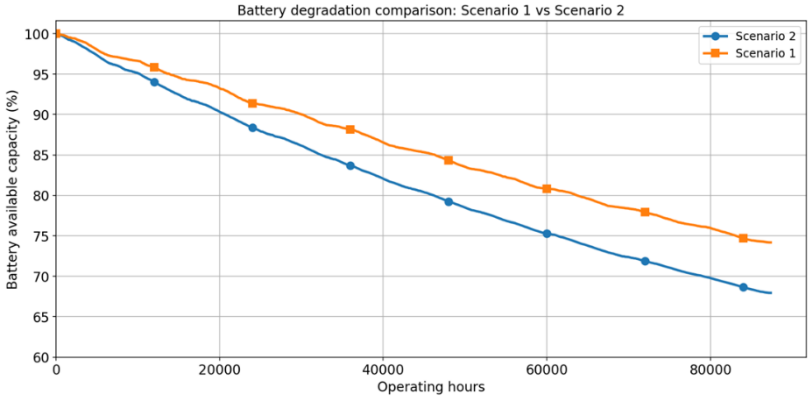

In Scenario 2, due to the structure of the proposed MILP framework, the battery is used more intensively to maintain the PEMWE within its most efficient operating region. This operating strategy enhances PEMWE efficiency, but at the same time causes faster BESS ageing and a significant reduction in its lifetime.
The resulting assessment of BESS ageing suggests a battery lifetime shorter than the value assumed in Section 2.3 (Table 3), which was used for the preliminary calculation of a LCOE equal to 75 €/MWh. When the estimated lifetime is taken into account, the LCOE increases by approximately 3% in Scenario 1 and by 6% in Scenario 2.
As for the battery degradation, Scenario 2 reports a higher degradation of the PEMWE compared to Scenario 1 due to the higher current densities reached during operation and the degradation function considered in Eq. (3).
Considering [25] the recommended EoL condition for the PEMWE stack is reached when the cell voltage at nominal load increases from 1.99 V BoL to 2.20 V, corresponding to an increase of about 10%.
Figure 3 shows the relationship between cumulative degradation and cumulative hydrogen production for the two operating scenarios.
The results are in line with literature for both Scenarios as the PEMWE reaches the EoL at approximately 70,000 h, therefore within the range of 20,000 – 80,000 hours identified by [34].
Scenario 1 lies above Scenario 2 over the whole time horizon, meaning that it reach a higher cumulative degradation to achieve the same cumulative hydrogen production. This reflects a less favourable degradation pattern for Scenario 1, because PEMWE degradation function represented in Eq. (30) is primarily associated with the cumulative operating time of the PEMWE.

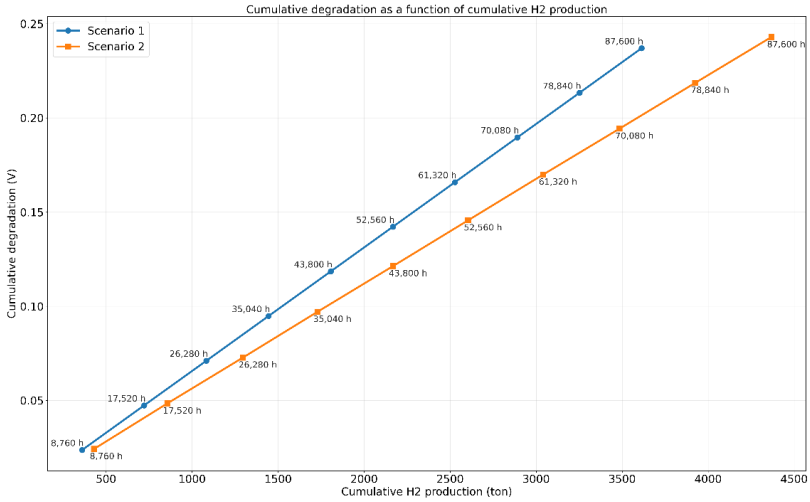

Figure 3: *Cumulative degradation as a function of cumulative H2 production.*

In contrast, Scenario 2 accumulates degradation slightly faster in absolute terms and therefore reaches the degradation threshold (0.2 V) earlier in terms of operational lifetime.
The different operating strategy adopted in Scenario 2 leads to an average increase in specific energy consumption of 1.34% compared to Scenario 1 when degradation is not considered. Moreover, when the effect

of degradation is included, this increase rises to 1.42%. This suggests that the difference between the two scenarios is primarily driven by the adopted operating strategy, while the contribution of degradation remains comparatively limited over the analyzed time horizon.
This effect becomes more evident in Figure 4, where the two curves represent the cost difference between the two operating scenarios when degradation is neglected (green curve) and when degradation is taken into account (red curve).

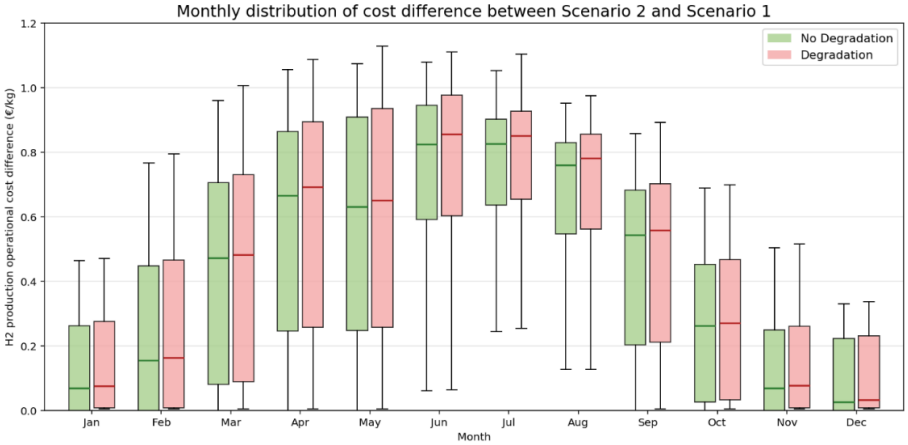

Figure 4: *Operational cost difference between Scenario 1 and Scenario 2 considering degradation (red) and non-considering the degradation (green)*

The monthly distribution of operational cost difference exhibits higher values during the summer period, as Scenario 2 relies more heavily on electricity imported from the grid, which is characterized by a higher unit energy cost. Overall, the cost increase reaches up to approximately 1 €/kg during the summer months and the resulting average annual increase in hydrogen production operational cost is about 6.2% in Scenario 2 compared to Scenario 1.

Conclusions

This work presents a system-level Mixed Integer Linear Programming (MILP) optimization framework for a long-term operation of a commercial-scale hydrogen production plant integrating water electrolysis, aimed at minimizing operational hydrogen production costs considering also BESS performance losses and evaluating PEMWE degradation over a hydrogen production time horizon of 87,600 h.
The results shows that the operating strategies, associated with different PPA contracts, significantly influences both the techno-economic performance of the plant and the ageing of the BESS and PEMWE.
In particular, Scenario 1, based on a fixed daily hydrogen production target with flexible grid support, results in a lower operational cost for hydrogen production. Scenario 2, by contrast, is characterized by a more intensive use of the BESS to keep the PEMWE operating closer to its highest-efficiency region, together with a slightly higher PEMWE degradation due to the higher operating loads reached.
The analysis highlighted that the BESS lifetime in Scenario 1 is approximately 25% higher than in Scenario 2. Therefore, a difference in LCOE of about 3% is expected between the two scenarios, due to the shorter BESS lifetime estimated for Scenario 2.
The inclusion of PEMWE degradation in the two operating scenarios results in an average increase in hydrogen production cost of 3.18% in Scenario 1 and 3.22% in Scenario 2 over the analyzed time horizon. The difference between the two scenarios remains limited because their annual average hydrogen production levels are relatively close, with Scenario 1 equal to 1000 kg/day and Scenario 2 equal to 1200 kg/day. However, under more demanding operating conditions, the impact of degradation on the overall hydrogen cost would become more significant.
Overall, the results highlight a clear trade-off between short-term operating efficiency and long-term system performance, showing that operating strategies aimed at maximizing PEMWE efficiency may not correspond to the most advantageous solution from a whole-system techno-economic perspective.
Future developments of the proposed framework will focus on extending the present formulation toward a multi-objective optimization approach, in which hydrogen production cost, PEMWE degradation, BESS ageing, and grid electricity utilization are simultaneously accounted.

Acknowledgments

The authors acknowledge the financial support of the North Adriatic Hydrogen Valley (NAHV) project, funded under the Horizon Europe programme (Grant Agreement ID: 101111927).

References

[1] A. Ursua, L. M. Gandia, and P. Sanchis, “Hydrogen Production From Water Electrolysis: Current Status and Future Trends,” *Proceedings of the IEEE*, vol. 100, no. 2, pp. 410–426, Feb. 2012, doi: 10.1109/JPROC.2011.2156750.

[2] G. Papakonstantinou, G. Algara-Siller, D. Teschner, T. Vidaković-Koch, R. Schlögl, and K. Sundmacher, “Degradation study of a proton exchange membrane water electrolyzer under dynamic operation conditions,” *Appl. Energy*, vol. 280, p. 115911, Dec. 2020, doi: 10.1016/j.apenergy.2020.115911.

[3] T. Khan, M. Yu, and M. Waseem, “Review on recent optimization strategies for hybrid renewable energy system with hydrogen technologies: State of the art, trends and future directions,” *Int. J. Hydrogen Energy*, vol. 47, no. 60, pp. 25155–25201, Jul. 2022, doi: 10.1016/j.ijhydene.2022.05.263.

[4] Y. Zheng, S. You, H. W. Bindner, and M. Münster, “Optimal day-ahead dispatch of an alkaline electrolyser system concerning thermal–electric properties and state-transitional dynamics,” *Appl. Energy*, vol. 307, p. 118091, Feb. 2022, doi: 10.1016/j.apenergy.2021.118091.

[5] E. N. Aminaho, N. S. Aminaho, and F. Aminaho, “Techno-economic assessments of electrolyzers for hydrogen production,” *Appl. Energy*, vol. 399, p. 126515, Dec. 2025, doi: 10.1016/j.apenergy.2025.126515.

[6] H. Zhang and T. Yuan, “Optimization and economic evaluation of a PEM electrolysis system considering its degradation in variable-power operations,” *Appl. Energy*, vol. 324, p. 119760, Oct. 2022, doi: 10.1016/j.apenergy.2022.119760.

[7] C. Campbell-Stanway, V. Becerra, and S. Prabhu, “Techno-economic analysis with electrolyser degradation modelling in green hydrogen production scenarios,” *Int. J. Hydrogen Energy*, vol. 106, pp. 80–95, Mar. 2025, doi: 10.1016/j.ijhydene.2025.01.359.

[8] “North Adriatic Hydrogen Valley (NAHV) testbed catalogue”, [Online]. Available: https://www.nahv.eu/testbeds-catalogue/

[9] G. Graber, V. Calderaro, V. Galdi, L. Ippolito, F. De Caro, and A. Vaccaro, “Day-Ahead Optimization of Proton Exchange Membrane Electrolyzer Operations Considering System Efficiency and Green Hydrogen Production Constraints Imposed by the European Regulatory Framework,” *Energies (Basel).*, vol. 17, no. 22, p. 5713, Nov. 2024, doi: 10.3390/en17225713.

[10] T. Egeland-Eriksen, A. Hajizadeh, and S. Sartori, “Hydrogen-based systems for integration of renewable energy in power systems: Achievements and perspectives,” *Int. J. Hydrogen Energy*, vol. 46, no. 63, pp. 31963–31983, Sep. 2021, doi: 10.1016/j.ijhydene.2021.06.218.

[11] T. Huld, R. Müller, and A. Gambardella, “A new solar radiation database for estimating PV performance in Europe and Africa,” *Solar Energy*, vol. 86, no. 6, pp. 1803–1815, Jun. 2012, doi: 10.1016/j.solener.2012.03.006.

[12] “Hydrogen Hyb Trieste - Sintesi non tecnica in formato digitale,” 2024, [Online]. Available: https://www.regione.fvg.it/rafvg/export/sites/default/RAFVG/ambiente-territorio/valutazione-ambientale-autorizzazioni-contributi/FOGLIA3/DITTE/allegati/TS_AIA_14_SNT.pdf

[13] International Energy Agency (IEA), “Projected Costs of Generating Electricity - 2020 edition,” 2020.

[14] Fraunhofer Institute for Solar Energy Systems (ISE), “Levelized Cost of Electricity Renewable Energy Technologies,” 2024.

[15] E. Vartiainen, G. Masson, C. Breyer, D. Moser, and E. Román Medina, “Impact of weighted average cost of capital, capital expenditure, and other parameters on future utility-scale PV levelised cost of electricity,” *Progress in Photovoltaics: Research and Applications*, vol. 28, no. 6, pp. 439–453, Jun. 2020, doi: 10.1002/pip.3189.

[16] J. Figgener *et al.*, “The development of stationary battery storage systems in Germany – A market review,” *J. Energy Storage*, vol. 29, p. 101153, Jun. 2020, doi: 10.1016/j.est.2019.101153.

[17] R. Vignesh, J. Zuboy, and M. Woodhouse, “U.S. Solar Photovoltaic System and Energy Storage Cost Benchmarks, With Minimum Sustainable Price Analysis: Q1 2023,” *NREL Technical Report*, 2023.

[18] D. Polverini, N. Dodd, and N. Espinosa, “Potential regulatory approaches on the environmental impacts of photovoltaics: Expected improvements and impacts on technological innovation,” *Progress*

in Photovoltaics: Research and Applications, vol. 29, no. 1, pp. 83–97, Jan. 2021, doi: 10.1002/pip.3344.

[19] IRENA, “Renewable Power Generation Costs in 2024,” 2025.

[20] L. Jinko SOlar Co., “Tiger Neo N-type 72HL4-BDV 560-580 Watt ; BIFACIAL MODULE WITH DUAL GLASS.” Accessed: Dec. 18, 2025. [Online]. Available: https://jinkosolar.eu/wp-content/uploads/JKM560-580N-72HL4-BDV-F3-EN.pdf

[21] W. Cole and A. Karmakar, “Cost Projections for Utility-Scale Battery Storage: 2023 Update.,” National Renewable Energy Laboratory (NREL), 2023.

[22] J. Kang, F. Yan, P. Zhang, and C. Du, “A novel way to calculate energy efficiency for rechargeable batteries,” *J. Power Sources*, vol. 206, pp. 310–314, May 2012, doi: 10.1016/j.jpowsour.2012.01.105.

[23] G. Matute, J. M. Yusta, J. Beyza, and L. C. Correas, “Multi-state techno-economic model for optimal dispatch of grid connected hydrogen electrolysis systems operating under dynamic conditions,” *Int. J. Hydrogen Energy*, vol. 46, no. 2, pp. 1449–1460, Jan. 2021, doi: 10.1016/j.ijhydene.2020.10.019.

[24] F. MARANGIO, M. SANTARELLI, and M. CALI, “Theoretical model and experimental analysis of a high pressure PEM water electrolyser for hydrogen production,” *Int. J. Hydrogen Energy*, vol. 34, no. 3, pp. 1143–1158, Feb. 2009, doi: 10.1016/j.ijhydene.2008.11.083.

[25] Plug Power, “Allagash Electrolyzer stack spec sheet”, [Online]. Available: https://www.plugpower.com/hydrogen/electrolyzer-hydrogen/electrolyzer-products/

[26] National Renewable Energy Laboratory (NREL), “MW-Scale PEM-Based Electrolyzers for RES Applications,” 2021, [Online]. Available: https://docs.nlr.gov/docs/fy21osti/79055.pdf

[27] A. S. Tijani, N. A. Binti Kamarudin, and F. A. Binti Mazlan, “Investigation of the effect of charge transfer coefficient (CTC) on the operating voltage of polymer electrolyte membrane (PEM) electrolyzer,” *Int. J. Hydrogen Energy*, vol. 43, no. 19, pp. 9119–9132, May 2018, doi: 10.1016/j.ijhydene.2018.03.111.

[28] R. Taccani, G. Maggiore, and D. Micheli, “Development of a Process Simulation Model for the Analysis of the Loading and Unloading System of a CNG Carrier Equipped with Novel Lightweight Pressure Cylinders,” *Applied Sciences*, vol. 10, no. 21, p. 7555, Oct. 2020, doi: 10.3390/app10217555.

[29] L. Gurobi Optimization, “Gurobi Optimizer Reference Manual,” 2024. [Online]. Available: https://www.gurobi.com

[30] F. Superchi, F. Papi, A. Mannelli, F. Balduzzi, F. M. Ferro, and A. Bianchini, “Development of a reliable simulation framework for techno-economic analyses on green hydrogen production from wind farms using alkaline electrolyzers,” *Renew. Energy*, vol. 207, pp. 731–742, May 2023, doi: 10.1016/j.renene.2023.03.077.

[31] Y. Shi, B. Xu, Y. Tan, D. Kirschen, and B. Zhang, “Optimal Battery Control Under Cycle Aging Mechanisms in Pay for Performance Settings,” *IEEE Trans. Automat. Contr.*, vol. 64, no. 6, pp. 2324–2339, Jun. 2019, doi: 10.1109/TAC.2018.2867507.

[32] A. Elizetxea-Navarro, J. Aizpuru, Y. Peña-Sanchez, M. Centeno-Telleria, A. Goikoetxea, and M. Penalba, “Assessing the impact of PEM electrolyser degradation for green hydrogen production: Power variability and ageing effects,” *Energy Convers. Manag.*, vol. 353, p. 121142, Apr. 2026, doi: 10.1016/j.enconman.2026.121142.

[33] J. Cai, H. Zhang, and X. Jin, “Aging-aware predictive control of PV-battery assets in buildings,” *Appl. Energy*, vol. 236, pp. 478–488, Feb. 2019, doi: 10.1016/j.apenergy.2018.12.003.

[34] A. Buttler and H. Spliethoff, “Current status of water electrolysis for energy storage, grid balancing and sector coupling via power-to-gas and power-to-liquids: A review,” *Renewable and Sustainable Energy Reviews*, vol. 82, pp. 2440–2454, Feb. 2018, doi: 10.1016/j.rser.2017.09.003.